Multifractal Analysis of Human Retinal Vessels

Tatijana Stošić and Borko D. Stošić*

***Abstract*—In this paper, it is shown that vascular structures of the human retina represent geometrical multifractals, characterized by a hierarchy of exponents rather then a single fractal dimension. A number of retinal images from the STARE database are analyzed, corresponding to both normal and pathological states of the retina. In all studied cases, a clearly multifractal behavior is observed, where capacity dimension is always found to be larger then the information dimension, which is in turn always larger then the correlation dimension, all the three being significantly lower then the diffusion limited aggregation (DLA) fractal dimension. We also observe a tendency of images corresponding to the pathological states of the retina to have lower generalized dimensions and a shifted spectrum range, in comparison with the normal cases.**

***Index Terms*—Blood vessels, fractals, multifractals, retina.**

I. Introduction

OVER the past decade, there have been several attempts [1]–[6] in the direction of employing the fractal dimension as a measure for quantifying the "state" of human retinal vessel structures (considered as geometrical objects), with the expectation that such analysis may contribute to automatic detection of pathological cases, and, therefore, to computerization of the diagnostic process. While this is certainly a valid question with possibly high impact on real world diagnostic issues, there are some issues that should be addressed before such investigations may prove useful for the standard clinical practice. First, the fact that retinal vessels represent "finite size" realizations of a fractal growth process, imposes questions about how exactly should one go about measuring the fractal dimension of a particular instance (e.g., an electronic image of a retinal vessel structure, taken from a given angle, with a given resolution and lightning conditions). A related question is to what extent these calculations may correspond to the limiting fractal (which would have been attained if the growth process could have been extended to infinity), or equivalently, to what degree they may be compared with calculations on other such finite instances. Although various issues related to these questions have already been addressed (for a current review, see, e.g., [6]), it seems that many of them remain open for further investigation. Second, some of these works [3], [4] address the point that the retinal vessels may have different properties in different regions, and do indeed find different characteristics depending on the locale of measurement, although the procedures adopted in these works are only remotely related to established concepts of multifractality, and the corresponding commonly accepted procedures for its measurement (see, e.g., [7]–[12] and references therein).

In this paper, we concentrate on the latter of the above issues, that is, we show that the human retinal vessel structures are geometrical multifractals, characterized by a hierarchy of exponents rather then a single fractal dimension. We analyze a number of retinal images from the STARE database [13], corresponding to both normal and pathological states of the retina. In all cases, we find clearly multifractal behavior. The capacity (or box counting) dimension is always found to be larger then the information (or Shannon) dimension, which is in turn always larger then the correlation dimension. In all cases, the observed values of the capacity dimension were significantly lower then the diffusion limited aggregation (DLA) fractal dimension, which has been considered in earlier works [1], [2], [6] as the primary model relevant for the phenomenon at hand. It is also found that images corresponding to pathological cases tend to have lower generalized dimensions, as well as a shifted spectrum range, in comparison with the normal cases.

II. Multifractal Analysis

In contrast to simple fractals (or monofractals), multifractals are characterized by a hierarchy of exponents, rather then a single fractal dimension. More precisely, multifractals may be viewed as a union of intervowen monofractals, embedded into each other. The word "hierarchy" here refers to different members of this union, which are characterized by distinct fractal dimensions. If this property is disregarded, and a multifractal object is treated as a simple (mono)fractal, the common methods for measuring fractal dimension yield some intermediate values, where typically the capacity dimension (which is measured, for example, by box counting method) turns out larger then the correlation dimension (measured by methods such as radius of gyration or the density–density correlation function). Therefore, the first test of multifractality may be performed by computing the capacity dimension and the correlation dimension, if they turn out to be different, one should proceed with the full multifractal spectrum analysis, as described below.

A well-known example of multifractality is the growth probability distribution during the DLA growth process, which has been shown to exhibit multifractal scaling [14]–[17]. Geometrical (or mass) multifractals represent a special case when the measure of interest is homogeneously distributed over the observed structure, so that only the number of particles (Lebesgue measure) contributes to the measure within a given region of the fractal [8], [9]. Considering a structure with mass (number of pixels) M_0 and linear size L, covered with a grid of boxes of

Manuscript received January 29, 2006; revised May 9, 2006. *Asterisk indicates corresponding author.*

T. Stošić is with the Departamento de Estatísica e Informática, Universidade Federal Rural de Pernambuco, Rua Dom Manoel de Medeiros s/n, Dois Irmaos, 52171-900 Recife-PE, Brazil.

*B. D. Stošić with the Departamento de Estatísica e Informática, Universidade Federal Rural de Pernambuco, Rua Dom Manoel de Medeiros s/n, Dois Irmaos, 52171-900 Recife-PE, Brazil (e-mail: borko@ufpe.br).

Digital Object Identifier 10.1109/TMI.2006.879316

linear size ℓ, the generalized dimension D_q for the mass distribution is defined by

$$\sum_i \left(\frac{M_i}{M_0}\right)^q \sim \left(\frac{\ell}{L}\right)^{(q-1)D_q} \quad (1)$$

where M_i is the mass (number of pixels) within the ith box, and q is a continuous (adjustable) variable that makes it possible to single out fractal properties of the object at different scales (equivalent of inverse temperature in thermodynamics). The generalized dimensions D_0, D_1, and D_2 correspond to the capacity (or box-counting) dimension, information (or Shannon) dimension, and correlation dimension, respectively. Finally, $D_{-\infty}$ and D_{∞} represent the limits of the generalized dimension spectrum, where the measure of interest is "most dilute" and "most dense," respectively. For monofractals, all the generalized dimensions coincide, being equal to the unique fractal dimension.

The multifractal spectrum is represented by the functional dependence $D(q)$, where for (mono)fractals of dimension D it is constant for all q $(D(q) = D)$, and for multifractals it is a monotone decreasing function of q. In the rest of this paper, we shall frequently refer to particular values D_0, D_1, and D_2 because they can be directly compared with the results of other works where the retinal vessel structures are treated as monofractals, however, they have no other special significance in comparison with D_q's for other values of q (each q corresponds to a particular level of density observed). Also, we shall repeatedly compare the numerical results for D_0 and D_2 (the most common monofractal measures) with the DLA fractal dimension estimate $D_{q=2} \simeq 1.71$ (commonly accepted in the literature) [9], as various earlier works [1], [2], [6] suggest that this extremely simple model [18] (random walkers attaching to a growing cluster, starting from a single initial seed) may be used to explain the retinal vessel structure formation, while our results indicate that this may be an oversimplification.

It turns out that the direct application of (1) in practice is hindered by the fact that for $q < 0$ the boxes that contain a small number of particles (because they barely overlap with the cluster) give anomalously large contribution to the sum on the left hand side of (1). To alleviate this problem and perform the multifractal analysis of the retinal vessel structures, we adopt the generalized sand box method [9], [10], which has been successfully used do demonstrate geometric multifractality of DLA [9]. This procedure consists in randomly selecting N of the M_0 points belonging to the structure, and counting for each such point i the number of pixels $M_i(R)$ that belong to the structure, inside boxes of growing linear dimension R, centered at the selected pixels. The quantity $M_i(R)/M_0$ may be understood as the empirical estimate of the spatial probability density of finding a pixel, belonging to the structure, at the position corresponding to the chosen point (it increases with the density of the tested region, it is greater then or equal to zero, and it sums to unity for a set of nonoverlapping boxes, of linear dimension R, fully covering the image). The left hand side of equation (1) can now be interpreted as the average of the quantity $(M_i(R)/M_0)^{q-1}$ according to spatial probability distribution $M_i(R)/M_0$. When the box centers are chosen randomly, the averaging should be made over the chosen set, and the equivalent of (1) becomes

$$\left\langle \left(\frac{M(R)}{M_0}\right)^{q-1} \right\rangle \sim \left(\frac{R}{L}\right)^{(q-1)D_q}. \quad (2)$$

Equation (2) represents only a very brief synthesis of the generalized sand box method [9], [10] (generally accepted in the literature dealing with multifractals), for more details, consult the original references. The practical advantage of this method is that the boxes are centered on the structure, so that by construction there are no boxes with too few particles (pixels) inside.

To verify whether human retinal vessel structures demonstrate geometrical multifractal scaling properties, we have used a set of forty retinal images from the STARE database [13], manually segmented by two different observers (from here referred to by initials AH and VK as in [13]) from twenty original retinal scans (containing ten normal and ten pathological cases), for the purpose of studies on automatic image segmentation and diagnosis [19]. The images segmented by observers AH and VK differ in level of detail, and the resulting set, totaling forty segmented images, is available for download from the STARE project [13] in ppm file format, with resolution of 700×605 pixels. As recently it has been argued [20] that fractal analysis may be more sensitive to changes in vascular patterns when skeletal images of vascular trees are considered, rather then the original segmented images (which contain the vessel width information), in order to verify whether the vessel width information indeed does exert influence on the multifractal analysis, we have also performed skeletonization of the two downloaded sets using the eight connected Rosenfeld algorithm [21], to produce two additional sets of 20 images each. A typical normal and a pathological image, segmented by observers AH and VK (where images segmented by observer VK demonstrate a substantially higher level of detail), respectively, together with their skeletonized versions using the Rosenfeld algorithm, are shown in Fig. 1.

It should be stressed at this point that the actual segmentation of retinal vessel images represents a formidable problem in itself, in particular because the absolute local intensity of the retinal images can vary according to a large number of factors (e.g., media opacity in the case of pathological subjects, screening technique, lightning conditions, etc.). As there seems to be no consensus yet in the literature as to automatic segmentation methods, we have chosen here to avoid altogether this problem, by using STARE database images *already segmented by trained individuals* (observers AH and VK). Results of this and other exploratory works may prove useful in practice only once that automatic segmentation methods are well established, and large (reliable) image databases of healthy and pathological subjects are constructed.

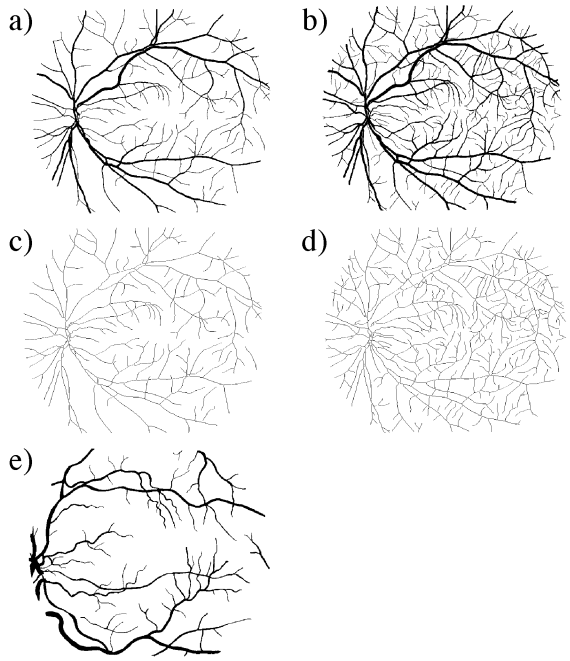

Fig. 1. Image of a typical normal retinal vessel structure (image files im0162.ah.ppm from the STARE database [13]), segmented by (a) observer AH and (b) observer VK, together with their skeletonized versions (c) and (d), respectively, and (e) a typical pathological structure (image file im0001.ah.ppm, diagnosed with Background Diabetic Retinopathy), segmented by observer AH.

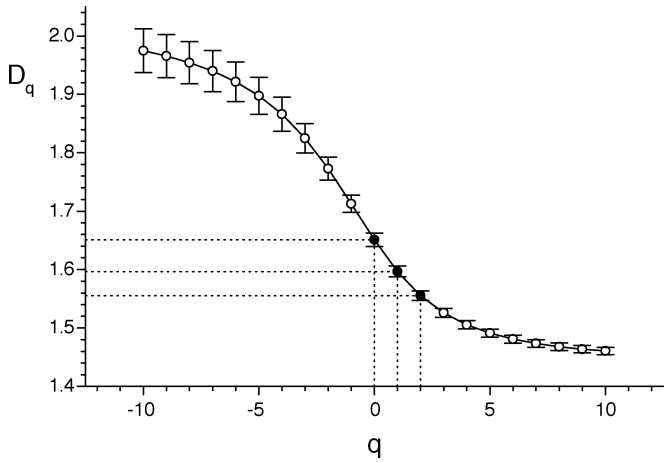

Fig. 2. Generalized dimension spectrum, D_q versus q, for a typical normal retinal image (image file im0162.ah.ppm [13]), averaged over 100 random choices of 1000 points each (see text for details). Error bars indicate $\pm 3\sigma$, with σ the standard deviation for the 100 runs at each q, and the curve connecting the points serves as a guide to the eye. Points corresponding to the capacity dimension $D_0 = 1.651$, the information dimension $D_1 = 1.597$ and the correlation dimension $D_2 = 1.555$ are represented by full circles, while the dotted lines serve to emphasize their position.

III. Results

A. Generalized Fractal Dimensions

For all of the four sets (containing 20 images each), we have performed measurements (calculations) according to (2), selecting 1000 random points on each structure (typical structure size M_0 is approximately 30 000 pixels, and the typical linear size L is 600 pixels), and counting number M_i of pixels inside boxes centered at selected points. These numbers were then used to extract generalized dimension D_q, for different values of q ($-10 < q < 10$), as slopes of the lines obtained through regression (minimum squares fitting) of $\log \langle [M(R)/M_0]^{q-1} \rangle / (q-1)$, as a function of $\log(R/L)$. The whole procedure was repeated 100 times (with different random choices of the 1000 random points), for each image, and for each value of q. The final values of D_q were calculated as averages over these repetitions.

A word is due on calculations for the special case $q = 1$, corresponding to information dimension D_1. As the above formulas are nonanalytic for $q = 1$, we perform calculations at $q = 1 \pm \epsilon$, for $\epsilon = 0.001$, and assuming linearity of the function $D(q)$ in this (short) interval, we interpolate $D_1 \approx (D_{1-\epsilon} + D_{1+\epsilon})/2$ (in fact, the difference between the values of D_q calculated on both sides of $q = 1$ was found to be only slightly larger then the statistical fluctuations induced by random choice of the set of measurement points on the structure).

Results of a typical calculation are shown in Fig. 2, where we display generalized dimension spectrum D_q versus independent parameter q, averaged over 100 random choices of 1000 points each. While there is no *a priori* reason why the calculations for a given value of q should follow any particular distribution, their binned frequency histograms reveal symmetric bell-shaped form, and the Shapiro–Wilk test [22] performed using DATAPLOT software package[1] accepts the normality assumption at the 99% level, in all cases. The error bars displayed in Fig. 2 were calculated as $\pm 3\sigma$, where σ is the standard deviation. The claim of this work (the null hypothesis H_0 in more formal statistical terms) is that the function $D(q)$ is a decreasing function of q (and, therefore, the vessel structure is a geometrical multifractal), rather than a constant (the vessel structure therefore being a simple fractal). As the error bars do not overlap on the full range of q, here we shall say that from the results displayed in Fig. 2 it is reasonable to conclude that the observed retinal vessel structure demonstrates multifractal scaling ($D(q)$ is a decreasing function of q), rather then being a simple monofractal ($D(q) = const.$), that is, we do not reject the null hypothesis. In particular, the capacity dimension D_0, the information dimension D_1 and the correlation dimension D_2 (values that may be compared with other works, which treat retinal vessel structures as simple fractal objects) are all different, satisfying $D_0 > D_1 > D_2$. Finally, all the three values remain substantially lower then the DLA fractal dimension estimate (commonly accepted in the literature) of $D_{q=2} \simeq 1.71$ (which is in fact underestimated by commonly used methods) [9]. This finding contradicts the previous works [1], [2], and [6], which claim that retinal vessel structures are fractals with the fractal dimension equal to that of the DLA, and, therefore, implicitly suggest that the mechanism responsible for formation of retinal vessel structures may be related to that of a DLA growth process. Our calculations show that all common measures of fractal dimension of the retinal vessels are well below their DLA equivalents, suggesting that the growth mechanism of the retinal vessels is different from that of the DLA.

[1]http://www.itl.nist.gov/div898/software/dataplot.html

TABLE I
GENERALIZED DIMENSIONS D_q, WITH STANDARD DEVIATION VALUES σ_q, FOR $q = -10$, 0, 1, 2, 10, FOR THE 20 ANALYZED IMAGES FROM THE STARE DATABASE. SECOND COLUMN INDICATES CLASSIFICATION STATUS FOR EACH OF THE IMAGES (PATHOLOGICAL OR NORMAL)

Image	Status	D_{-10}	σ_{-10}	D_0	σ_0	D_1	σ_1	D_2	σ_2	D_{10}	σ_{10}
im0001.ah	P	1.967	0.016	1.539	0.004	1.493	0.003	1.462	0.003	1.361	0.003
im0002.ah	P	1.928	0.018	1.549	0.004	1.498	0.003	1.460	0.003	1.370	0.002
im0003.ah	P	1.880	0.020	1.508	0.005	1.468	0.003	1.442	0.003	1.378	0.002
im0004.ah	P	1.784	0.025	1.522	0.003	1.491	0.003	1.464	0.003	1.366	0.002
im0005.ah	P	1.894	0.014	1.590	0.003	1.561	0.002	1.539	0.002	1.476	0.002
im0044.ah	P	1.886	0.014	1.540	0.004	1.493	0.003	1.458	0.003	1.362	0.002
im0077.ah	N	1.912	0.012	1.578	0.004	1.530	0.003	1.498	0.003	1.426	0.002
im0081.ah	N	1.914	0.017	1.554	0.003	1.514	0.003	1.487	0.002	1.422	0.002
im0082.ah	N	1.977	0.011	1.578	0.004	1.518	0.003	1.477	0.003	1.404	0.002
im0139.ah	P	1.919	0.027	1.565	0.004	1.516	0.003	1.482	0.003	1.414	0.002
im0162.ah	N	1.975	0.012	1.651	0.004	1.597	0.003	1.555	0.003	1.460	0.002
im0163.ah	N	1.989	0.018	1.641	0.005	1.586	0.003	1.550	0.002	1.475	0.001
im0235.ah	N	1.950	0.013	1.598	0.004	1.548	0.003	1.514	0.002	1.442	0.002
im0236.ah	N	1.882	0.015	1.585	0.003	1.545	0.003	1.515	0.002	1.448	0.002
im0239.ah	N	1.952	0.017	1.588	0.004	1.550	0.003	1.520	0.003	1.439	0.002
im0240.ah	N	1.918	0.019	1.594	0.003	1.565	0.002	1.544	0.002	1.495	0.002
im0255.ah	N	1.947	0.017	1.634	0.002	1.604	0.002	1.583	0.002	1.522	0.002
im0291.ah	P	1.818	0.026	1.519	0.004	1.483	0.004	1.455	0.003	1.347	0.003
im0319.ah	P	1.704	0.025	1.444	0.005	1.410	0.004	1.382	0.004	1.299	0.003
im0324.ah	P	1.923	0.022	1.567	0.004	1.520	0.003	1.486	0.002	1.399	0.001

Numerical results corresponding to Fig. 2 (for the set of twenty images from the STARE database segmented by observer AH) are given in Table I. The first column lists the image names, while the second column indicates image classification status as "pathological" or "normal."[2] The values of generalized dimensions D_q are given for $q = -10, 0, 1, 2, 10$, where as already mentioned D_0, D_1, and D_2 correspond to the capacity, information and correlation dimension, respectively, while D_{-10} and D_{10} indicate the range of the general dimension spectrum. It is seen from Table I that all of the values calculated for the capacity dimension (which corresponds to box counting method), and indeed the correlation dimension (corresponding to methods such as radius of gyration or the density–density correlation function), are significantly lower then the DLA fractal dimension $D_{q=2} \simeq 1.71$ [9]. Therefore, our results show that retinal vessel structures are geometrical multifractals, and that the overall fractal dimension is lower then that of the DLA.

Results of the multifractal analysis for the other three sets of images (STARE database images segmented by observer VK, and the skeletonized versions of AH and VK) all yield qualitatively similar results, all of them clearly demonstrating multifractal behavior. In Table II we present the results for the capacity (box counting) dimension D_0, for all of the four sets of images. It follows from Table II that the process of skeletonization (removal of vessel width information from the image) slightly reduces the fractal dimension, while this effect is much weaker in comparison with the effect of the level of detail present in the segmentation process, as found between the two current observers. However, when the results are compared consistently within each group separately, the mean fractal dimension is found to be lower for the pathological images then for the normal cases, for all of the four groups. Although this finding can hardly be considered conclusive from the statistical viewpoint, it is nevertheless encouraging from the point of view that fractal spectrum analysis could be employed for quantification of the retinal vessel state, in order to contribute to automatic diagnostics. To this end, far more detailed studies of images corresponding to specific diseases and normal cases, are needed. Assuming that each of the observers consistently applied his own criteria in segmentation, it follows that the fractal dimension results may be compared only between images segmented by the same observer, either skeletonized or not, but should be normalized before making comparisons of results from different groups.

[2]For more details on the diagnostic procedure used for classification of images, see http://www.parl.clemson.edu/stare/diagnoses

B. The $f(\alpha)$ Spectrum

When addressing multifractality, numerous works deal with the so-called $f(\alpha)$ spectrum (see, e.g., [7], [8], [23], and references therein), where

$$N(\alpha) = L^{-f(\alpha)} \tag{3}$$

represents the number of boxes $N(\alpha)$ such that the probability P_i of finding a particle (pixel) within a given region i scales as

$$P_i = L^{\alpha_i} \tag{4}$$

and $f(\alpha)$ may be understood as the fractal dimension of the union of regions with singularity strengths between α and $\alpha + d\alpha$. The exponent α takes values from the interval $[-\infty, \infty]$,

TABLE II
CAPACITY (OR BOX COUNTING) DIMENSION D_0 FOR THE TWO SETS OF IMAGES FROM THE STARE DATABASE SEGMENTED BY OBSERVERS AH AND VK, TOGETHER WITH THEIR SKELETONZIED VERSIONS. SECOND COLUMN INDICATES CLASSIFICATION STATUS FOR EACH OF THE IMAGES (PATHOLOGICAL OR NORMAL), AND THE LAST THREE LINES PRESENT AVERAGES FOR THE PATHOLOGICAL, NORMAL, AND ALL IMAGES, RESPECTIVELY

		AH		AH-S		VK		VK-S	
Image	Status	D_0	σ_0	D_0	σ_0	D_0	σ_0	D_0	σ_0
im0001.ah	P	1.539	0.004	1.544	0.004	1.584	0.004	1.594	0.004
im0002.ah	P	1.549	0.004	1.524	0.005	1.574	0.005	1.570	0.004
im0003.ah	P	1.508	0.005	1.500	0.005	1.595	0.004	1.608	0.004
im0004.ah	P	1.522	0.003	1.510	0.005	1.573	0.005	1.599	0.004
im0005.ah	P	1.590	0.003	1.553	0.004	1.680	0.003	1.664	0.003
im0044.ah	P	1.540	0.004	1.539	0.004	1.667	0.003	1.661	0.003
im0077.ah	N	1.578	0.004	1.590	0.004	1.659	0.002	1.661	0.003
im0081.ah	N	1.554	0.003	1.551	0.004	1.668	0.003	1.670	0.003
im0082.ah	N	1.578	0.004	1.584	0.004	1.666	0.003	1.679	0.002
im0139.ah	P	1.565	0.004	1.564	0.004	1.679	0.005	1.677	0.007
im0162.ah	N	1.651	0.004	1.637	0.003	1.714	0.002	1.700	0.002
im0163.ah	N	1.641	0.005	1.612	0.003	1.685	0.002	1.647	0.003
im0235.ah	N	1.598	0.004	1.586	0.004	1.683	0.002	1.674	0.003
im0236.ah	N	1.585	0.003	1.585	0.004	1.658	0.003	1.660	0.003
im0239.ah	N	1.588	0.004	1.594	0.004	1.656	0.003	1.655	0.003
im0240.ah	N	1.594	0.003	1.564	0.005	1.675	0.003	1.664	0.002
im0255.ah	N	1.634	0.002	1.634	0.003	1.696	0.002	1.692	0.002
im0291.ah	P	1.519	0.004	1.491	0.006	1.603	0.010	1.581	0.017
im0319.ah	P	1.444	0.005	1.450	0.005	1.554	0.004	1.564	0.003
im0324.ah	P	1.567	0.004	1.506	0.005	1.644	0.004	1.617	0.003
Average	P	1.534	0.013	1.518	0.015	1.615	0.016	1.614	0.021
	N	1.600	0.012	1.593	0.012	1.677	0.008	1.672	0.008
	All	1.567	0.017	1.556	0.019	1.646	0.018	1.642	0.023

and the function $f(\alpha)$ is usually a single humped function with a maximum at $df(\alpha)/d\alpha = 0$. The relationship between the $D(q)$ spectrum and the $f(\alpha)$ spectrum is made via the Legendre transform

$$f(\alpha(q)) = q\alpha(q) - \tau(q) \tag{5}$$

where

$$\alpha(q) = \frac{d\tau(q)}{dq} \tag{6}$$

and

$$\tau(q) \equiv (q-1)D_q \tag{7}$$

is the mass correlation exponent of the qth order. In the limiting case of a simple fractal (monofractal), the fractal dimension is independent of q ($D_q \equiv D$), from (6) and (7) it follows that $\alpha(q) = D$, and finally from (5) and (7) it follows that $f(\alpha) = D$. Monofractal structures should be, therefore, represented by a single point $f(\alpha) = \alpha = D$ on the $f(\alpha)$ scatterplot, while multifractal structures produce a nontrivial spectrum.

To address the question of multifractality of retinal vessel structures within this framework, in Fig. 3 we present the $f(\alpha)$ spectrum for a typical normal retinal image (image file im0162.ah.ppm [13]). To calculate the derivatives in (6), we have performed calculations at pairs of points q and $q + \epsilon$ with $\epsilon = 0.001$, so that derivatives were calculated as $d\tau(q)/dq \approx (\tau(q+\epsilon) - \tau(q))/\epsilon$, except at point $q = 1$, where we have used $d\tau(q)/dq \approx (\tau(1+\epsilon) - \tau(1-\epsilon))/(2\epsilon)$. As before, the Shapiro–Wilks test [22] was performed using DATAPLOT software package[1] to check the distribution of α and $f(\alpha)$ over the 100 repetitions at each q [the same that were used to evaluate the $D(q)$], and as before the test accepts the normality assumption at the 99% level, in all cases. The standard deviation was then calculated for each α and each

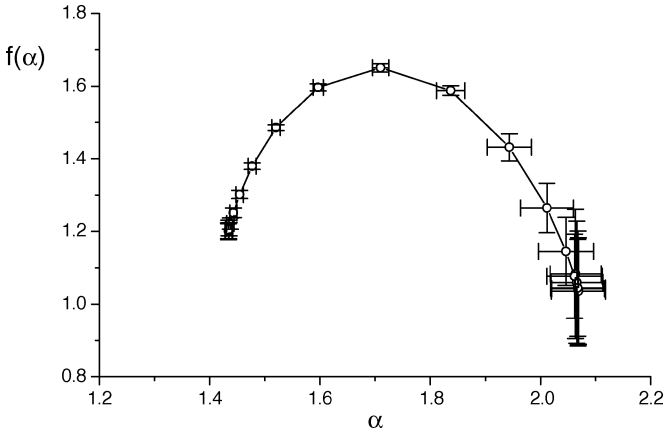

Fig. 3. The $f(\alpha)$ spectrum for a typical normal retinal image (image file im0162.ah.ppm [13]), with the error bars corresponding to $\pm 3\sigma$ (σ being the standard deviation over the 100 runs for each point, see text for more details).

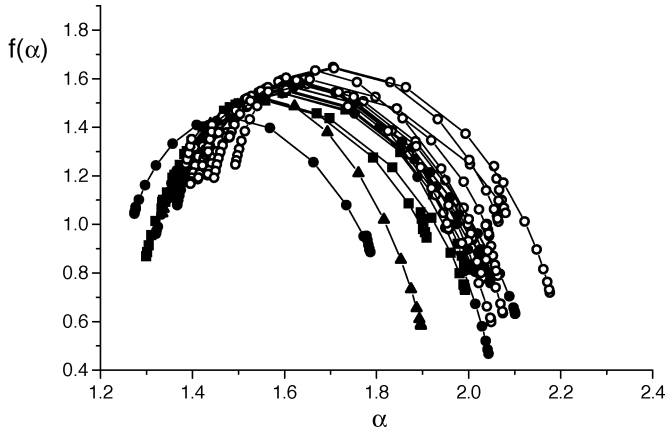

Fig. 4. The $f(\alpha)$ spectrum for the 20 images from the STARE database [13], segmented by observer AH. Curves corresponding to normal retinal images are represented by open circles, and those corresponding to pathological images[2] are represented by full symbols. It is seen that pathological image curves tend to be shifted to the lower α range and have lower maxima, in comparison with the normal images (see text for more details).

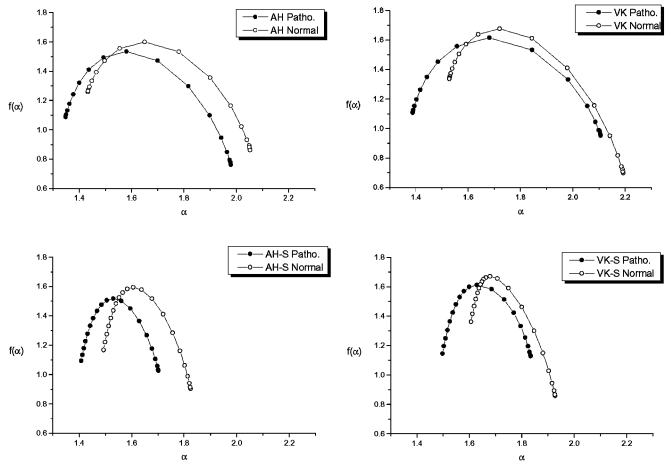

Fig. 5. The $f(\alpha)$ spectrum for the 20 images from the STARE database [13], segmented by observer AH. Curves corresponding to normal retinal images are represented by open circles, and those corresponding to pathological images[2] are represented by full symbols. It is seen that pathological image curves tend to be shifted to the lower α range and have lower maxima, in comparison with the normal images (see text for more details).

$f(\alpha)$ from the repetitions. The error bars displayed in Fig. 3 have triple magnitude of these standard deviation values, and as they do not overlap across the entire spectrum, again we may conclude that the retinal vessel structures exhibit multifractal scaling (we do not reject the null hypothesis).

In Fig. 4, we show detailed results of our calculations, performed on the STARE database images segmented by observer AH, with respect to the $f(\alpha)$ spectrum. While the current set of images is not particularly adequate for testing the effects of a given type of pathology (there are only ten normal images, and ten pathological images affected by not necessarily the same disease[2]), it is seen that pathological case images tend to have lower maxima, occasionally more narrow spectrum range, and a shift in the spectrum position, in comparison with the normal cases.

Finally, in Fig. 5, we present results of the $f(\alpha)$ spectrum averaged separately for the normal and the pathological images for all of the four sets, where it is seen that the previous observation holds for both observers, independent of skeletonization. The skeletonized images present more narrow $f(\alpha)$ spectrum then the original segmented images (which contain the vessel width information) for both observers, which may explain the conclusion of [20] that fractal analysis after skeletonization may be more sensitive to changes in vascular patterns. More precisely, since monofractals have infinitely narrow $f(\alpha)$ spectrum (a single fractal dimension), the above results show that skeletonized structures may be more closely approximated as monofractals (when a single dimension is calculated rather then the whole spectrum). As the general properties of the spectrum are preserved through skeletonization, another advantage of using such images may be considered the fact that they contain far fewer pixels, and, therefore, the calculations require less computer time.

The results of calculations of the $f(\alpha)$ spectrum presented in Figs. 4 and 5 again may be considered encouraging from the point of view of the objective of turning the diagnostic process automatic, although further more detailed studies are necessary to determine their statistical significance, and whether the observed differences in multifractal scaling behavior may be exploited for discerning normal images from images with certain types of pathologies. More precisely, the current work is primarily concerned with establishing the fact that retinal vessel images represent geometrical multifractals, nevertheless, our calculations suggest that there may be grounds for automatic differentiating between normal images and certain pathological cases.

IV. Conclusion

In conclusion, we show in this paper that vascular structures of the human retina represent geometrical multifractals, characterized by a hierarchy of exponents, rather then a single fractal dimension. We analyze 20 retinal images from the STARE database [13], where half of the images correspond to normal states of the retina, and half to different pathological states,[2] together with their skeletonized versions. In all studied cases we find clearly multifractal behavior, with capacity dimension considerably lower then the DLA value. We also observe a tendency of normal images of having higher generalized dimensions and a shift of the $f(\alpha)$ spectrum range towards higher singularity strength values, in comparison with the pathological cases. While the last observations are hardly conclusive from a statistical standpoint, they may prove relevant in the quest of automatic diagnostic procedures.

Acknowledgment

The authors would like to thank the STARE project group for making the database publicly available, and the anonymous referees for constructive criticism.

References

[1] F. Family, B. R. Masters, and D. E. Platt, "Fractal pattern formation in human retinal vessels," *Physica D*, vol. 38, pp. 98–103, 1989.
[2] M. A. Mainster, "The fractal properties of retinal vessels: Embryological and clinical implications," *Eye*, vol. 4, pp. 235–241, 1990.
[3] G. Landini, P. I. Murray, and G. P. Misson, "Local connected fractal dimensions and lacunarity analyses of 60 ° fluorescein angiograms," *Invest. Ophtal. Vis. Sci.*, vol. 36, pp. 2749–2755, 1995.

[4] A. Avakian, R. E. Kalina, H. E. Sage, A. H. Rambhia, K. E. Elliott, E. L. Chuang, J. I. Clark, J.-N. Hwang, and P. Parsons-Wingerter, "Fractal analysis of region-based vascular change in the normal and non-proliferative diabetic retina," *Curr. Eye. Res.*, vol. 24, pp. 274–280, 2002.

[5] V. Lakshminanarayanan, A. Raghuram, J. W. Myerson, and S. Varadharajan, "The fractal dimension in retinal pathology," *J. Mod. Opt.*, vol. 50, pp. 1701–1704, 2003.

[6] B. R. Masters, "Fractal analysis of the vascular tree in the human retina," *Ann. Rev. Bio. Eng.*, vol. 6, pp. 427–452, 2004.

[7] J. Feder, *Fractals*. New York: Plenum, 1988.

[8] T. Vicsek, *Fractal Growth Phenomena*, 2nd ed. Singapore: World Scientific, 1993.

[9] T. Vicsek, F. Family, and P. Meakin, "Multifractal geometry of diffusion-limited aggregates," *Europhys. Lett.*, vol. 12, pp. 217–222, 1990.

[10] T. Tél, A. Füllöp, and T. Vicsek, "Determination of fractal dimensions for geometrical multifractals," *Physica A*, vol. 159, pp. 155–166, 1989.

[11] A. Chhabra and R. V. Jensen, "Direct determination of the f(alpha) singularity spectrum," *Phys. Rev. Lett.*, vol. 62, pp. 1327–1330, 1989.

[12] A. B. Chhabra, C. Meneveau, R. V. Jensen, and K. R. Sreenivasan, "Direct determination of the f(alpha) singularity spectrum and its application to fully developed turbulence," *Phys. Rev. A*, vol. 40, pp. 5284–5294, 1989.

[13] The STructured Analysis of the Retina (STARE) Project [Online]. Available: www.parl.clemson.edu/stare/probing Last seen on, Oct. 8, 2005

[14] C. Amitrano, A. Coniglio, and F. di Liberto, "Growth probability distribution in kinetic aggregation processes," *Phys. Rev. Lett.*, vol. 57, pp. 1016–1019, 1986.

[15] Y. Hayakawa, S. Sato, and M. Matsushita, "Scaling structure of the growth-probability distribution in diffusion-limited aggregation processes," *Phys. Rev. A*, vol. 36, pp. 1963–1966, 1987.

[16] J. Nittmann, H. E. Stanley, E. Torboul, and G. Daccord, "Experimental evidence for multifractality," *Phys. Rev. Lett.*, vol. 58, p. 619, 1987.

[17] S. Ohta and H. Honjo, "Growth probability distribution in irregular fractal-like crystal growth of ammonium chloride," *Phys. Rev. Lett.*, vol. 60, pp. 611–614, 1988.

[18] T. A. Witten and L. M. Sander, "Diffusion-limited aggregation: A kinetic critical phenomenon," *Phys. Rev. Lett.*, vol. 47, pp. 1400–1403, 1981.

[19] A. Hoover, V. Kouznetsova, and M. Goldbaum, "Locating blood vessels in retinal images by piece-wise threhsold probing of a matched filter response," *IEEE Trans. Med. Imag.*, vol. 19, no. 3, pp. 203–210, Mar. 2000.

[20] P. Parsons-Wingerter, K. E. Elliott, J. I. Clark, and A. G. Farr, "Fibroblast growth factor-2 selectively stimulates angiogenesis of small vessels in arterial tree," *Arteriosler. Thromb. Vasc. Biol.*, vol. 20, pp. 1250–1256, 2000.

[21] S. Stefanelli and A. Rosenfeld, "Some parallel thinning algorithms for digital pictures," *J. Assoc. Comput. Mach.* , vol. 18, pp. 255–264, 1971.

[22] S. S. Shapiro and M.B. Wilk, "An analysis of variance test for normality," *Biometrika*, vol. 52, no. 3, pp. 591–599, 1965.

[23] T. C. Halsey, M. H. Jensen, L. P. Kadanoff, I. Procaccia, and B. I. Shraiman, "Fractal measures and their singularities: The characterization of strange sets," *Phys. Rev. A*, vol. 33, pp. 1141–1151, 1986.